Voltage-controlled colour-tunable microcavity OLEDs with enhanced colour purity

2008 J. Phys. D: Appl. Phys. 41 025106

(http://iopscience.iop.org/0022-3727/41/2/025106)

IOP PUBLISHING JOURNAL OF PHYSICS D: APPLIED PHYSICS

J. Phys. D: Appl. Phys. **41** (2008) 025106 (5pp) doi:10.1088/0022-3727/41/2/025106

Voltage-controlled colour-tunable microcavity OLEDs with enhanced colour purity

Wallace C H Choy[1,3], J H Niu[1,2], W L Li[2] and P C Chui[1]

[1] Department of Electrical and Electronic Engineering, University of Hong Kong, Pokfulam Road, Hong Kong

[2] Changchun Institute of Optics, Fine Mechanics and Physics, Chinese Academy of Sciences, Changchun 130033, People's Republic of China

E-mail: chchoy@eee.hku.hk

Received 9 July 2007, in final form 3 December 2007
Published 21 December 2007
Online at stacks.iop.org/JPhysD/41/025106

Abstract

The emission spectrum of single-unit voltage-controlled colour-tunable organic light emitting devices (OLEDs) has been theoretically and experimentally studied. Our results show that by introducing the microcavity structure, the colour purity of not only the destination colour but also the colour-tunable route can be enhanced, while colour purity is still an issue in typical single-unit voltage-controlled colour-tunable OLEDs. With the consideration of the periodical cycling of resonant wavelength and absorption loss of the metal electrodes, the appropriate change in the thickness of the microcavity structure has been utilized to achieve voltage-controlled red-to-green and red-to-blue colour-tunable OLEDs without adding dyes or other organic materials to the OLEDs.

1. Introduction

Colour tunability by controlling the bias voltage can provide an extra degree of freedom for organic light emitting devices (OLEDs) to improve the performance and explore new potential applications. Various device structures have been used to achieve real-time colour tunability of OLEDs. A stacked device structure composed of two or three light emitting device units can realize real-time colour-tunable OLEDs [1–3]. The selection of colour is obtained by simply controlling the bias of each device unit. However, the number of layers of the two or three colour-tunable OLEDs is almost double or triple that of conventional OLEDs, respectively, which makes the device difficult to fabricate and easily introduces inherent optical resonance effects. In addition, the semitransparent intermediate electrodes between adjacent units, which are composed of a thin metal layer and a transparent indium-tin oxide (ITO) thin film for electron- and hole-injection, respectively, are difficult to fabricate, in particular, the ITO. On the other hand, single-unit real-time colour-tunable OLEDs have been reported. Two or more organic materials (small molecules [4–6] or polymers [7–9]) with various spectral energy distributions have been used in a single device unit and the response for emitting the tunable colour obtained by varying the applied voltage. However, the emission spectrum is usually relatively broad and the colour purity needs improvement.

In this paper, our focus is on the study of the light emission properties of single-unit real-time colour-tunable OLEDs, operated by changing the applied voltage, with the aim of improving the colour purity and widening the colour-tunable routes. Both theoretical and experimental works are conducted in this study. For modelling of OLEDs, light emits at the emitting region inside the multilayered structures. We will study the light emission properties by using the classical electromagnetic approach with the power radiated by a classical Hertz dipole in the recombination zone. In our model, a comprehensive consideration of the Purcell effect [10] due to the Fabry–Perot structure [11] of microcavity OLEDs, the nonradiative losses due to metal electrodes [12] and other materials as well as the effects of a thick glass substrate have been taken into account which have not been fully addressed by some recent reports [13–15]. We have recently reported the use of tris(dibenzoylmethanato) (bathophenanthroline) europium

[3] Author to whom any correspondence should be addressed.

(Eu(DBM)$_3$bath) as a good starting point close to the red corner of the CIE chromaticity diagram for wide colour tuning [16]. However, blue or green emission of colour-tunable OLEDs by using dyes is still broad. Here, we introduce an appropriate cavity structure not only to narrow down the emission spectrum but also to engineer the destination colour to blue or green without introducing extra light emitting materials to the device; yet red colour emission of the Eu(DBM)$_3$bath at low bias is maintained for achieving voltage-controlled red-to-green or -blue colour-tunable OLEDs with improved colour purity.

2. Experiment and modelling

The basic structure (Device A) of the colour-tunable device is ITO/Ag(x nm)/copper phthalocyanine (CuPc) (10 nm)/N, N′-di(1-naphthyl)-N, N′-diphenyl-1, 1′-diphenyl-1,4′-diamine) (NPD) (50 nm)/Eu(DBM)$_3$bath (20 nm)/tris(8-hydroxy quinolinato) aluminium (Alq_3) (40 nm)/LiF (0.5 nm)/Al (150 nm). NPD is used as the blue emitter and hole transporting layer. Alq_3 is used as the electron transporting layer. Besides the use of the Ag layer to form the microcavity structure, the emission colour is tuned by modifying the thickness of NPD in Device B: ITO/Ag(40 nm)/CuPc(10 nm)/NPD(x nm)/Eu(DBM)$_3$bath (15 nm)/Alq_3 (25 nm)/LiF (0.5 nm)/Al (150 nm). The organic materials were purified by gradient sublimation prior to thin-film coating when the Eu(DBM)$_3$bath was used without further purification. All the organic materials and the Ag and LiF/Al electrodes are deposited by conventional thermal vacuum deposition at a pressure of 10^{-6} Torr. The deposition rates for organic materials and Ag were typically 1.0–2.0 Å s^{-1}. The deposition rates of LiF and Al were 0.1 Å s^{-1} and 10–15 Å s^{-1}, respectively. The film thickness was monitored *in situ* using the quartz crystal monitor and *ex situ* by a stylus profilometer (Tencor α-step 500). The emission area of the devices is 4.57 mm^2. Details of the fabrication steps can also be found elsewhere [17]. Using a monochromator (Acton SpectraPro 275) for the wavelength selection, the spectrum was detected by a photomultiplier (Hamamatsu R636-10 PMT with a response time of nanoseconds) and the OLEDs were biased by using a programmable Keithley source meter 2400.

In order to understand the colour tuning spectrum and design the cavity structures, the light emission of multilayered OLED structures is rigorously modelled through a classical approach with an emitting layer sandwiched between two stacks of films (M layers above and N layers below). The vertical electric dipole (VED) and horizontal electric dipole (HED) are located in the recombination zone with distances Z_+ and Z_- from the top and bottom interfaces of the emitting layer, respectively, as shown in figure 1. The two stacks of films above and below the emitting layer can be considered as two effective interfaces characterized by the total reflection and transmission coefficients $r^{\mathrm{TM/TE}}_{e,M/-N}$ and $t^{\mathrm{TM/TE}}_{e,M/-N}$. Starting from the outermost layer, the total reflection and transmission coefficients can be obtained by iteratively

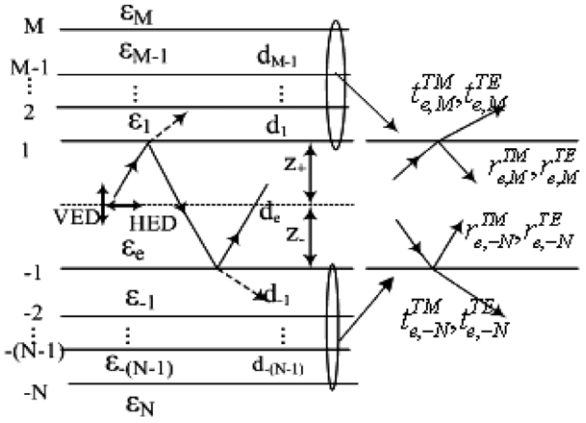

Figure 1. A planar multilayer OLED consisting of an emitting layer and two film stacks with relative permittivity and thickness of (ε_i, d_i) $(i = -N, \ldots, -1, e, 1, \ldots, M)$ for each layer. VED and HED are located in the emitting layer with distances Z_+ and Z_- from the layer with notations of 1 and -1. The simplified structure described by $r^{\mathrm{TM/TE}}_{e,M/-N}$ and $t^{\mathrm{TM/TE}}_{e,M/-N}$ is shown on the right-hand side.

calculating

$$r^{\mathrm{TM/TE}}_{i,M/-N} = \frac{r^{\mathrm{TM/TE}}_{i,i\pm1} + r^{\mathrm{TM/TE}}_{i\pm1,M/-N}\exp(2\mathrm{j}k_{z,i\pm1}d_{i\pm1})}{1 + r^{\mathrm{TM/TE}}_{i,i\pm1} \times r^{\mathrm{TM/TE}}_{i\pm1,M/-N}\exp(2\mathrm{j}k_{z,i\pm1}d_{i\pm1})}, \quad (1)$$

$$t^{\mathrm{TM/TE}}_{i,M/-N} = \frac{t^{\mathrm{TM/TE}}_{i,i\pm1} \times t^{\mathrm{TM/TE}}_{i\pm1,M/-N}\exp(2\mathrm{j}k_{z,i\pm1}d_{i\pm1})}{1 + r^{\mathrm{TM/TE}}_{i,i\pm1} \times r^{\mathrm{TM/TE}}_{i\pm1,M/-N}\exp(2\mathrm{j}k_{z,i\pm1}d_{i\pm1})}, \quad (2)$$

with

$$r^{\mathrm{TM/TE}}_{M,M} = 0, r^{\mathrm{TM/TE}}_{-N,-N} = 0,$$
$$r^{\mathrm{TM}}_{i,i\pm1} = (k_{z,i}\varepsilon_{i\pm1} - k_{z,i\pm1}\varepsilon_i)/(k_{z,i}\varepsilon_{i\pm1} + k_{z,i\pm1}\varepsilon_i),$$
$$r^{\mathrm{TE}}_{i,i\pm1} = (k_{z,i} - k_{z,i\pm1})/(k_{z,i} + k_{z,i\pm1}),$$
$$t^{\mathrm{TM/TE}}_{i,i\pm1} = 1 + r^{\mathrm{TM/TE}}_{i,i\pm1},$$

where $i = M, M-1, \ldots, 2, 1$ or e layer or $i = -N, -N+1, \ldots, -2, -1$ or e layer. $r^{\mathrm{TM}}_{i,i\pm1}$ ($r^{\mathrm{TE}}_{i,i\pm1}$) is the amplitude reflection coefficient of a TM (TE) polarized plane wave in the medium ε_i on an adjacent medium $\varepsilon_{i\pm1}$, respectively. $t^{\mathrm{TM}}_{i,i\pm1}$ ($t^{\mathrm{TE}}_{i,i\pm1}$) is the amplitude transmission coefficient of a TM (TE) polarized wave, respectively.

The total radiation power F_{V} and F_{H} for VED and HED, respectively, normalized by the radiation power of the dipole in an infinite medium ε_e, can be obtained [10, 18, 19]:

$$F_{\mathrm{V}} = \int_0^\infty \Re\left[\frac{3k_\rho^2(1 + r^{\mathrm{TM}}_{e,M}\mathrm{e}^{2\mathrm{j}k_{z,e}z_+})(1 + r^{\mathrm{TM}}_{e,-N}\mathrm{e}^{2\mathrm{j}k_{z,e}z_-})}{4k_{z,e}k_e^3(1 - r^{\mathrm{TM}}_{e,M}r^{\mathrm{TM}}_{e,-N}\mathrm{e}^{2\mathrm{j}k_{z,e}d_e})}\right]\mathrm{d}(k_\rho^2), \quad (3)$$

$$F_{\mathrm{H}} = \int_0^\infty \Re\left[\frac{3k_{z,e}(1 - r^{\mathrm{TM}}_{e,M}\mathrm{e}^{2\mathrm{j}k_{z,e}z_+})(1 - r^{\mathrm{TM}}_{e,-N}\mathrm{e}^{2\mathrm{j}k_{z,e}z_-})}{8k_e^3(1 - r^{\mathrm{TM}}_{e,M}r^{\mathrm{TM}}_{e,-N}\mathrm{e}^{2\mathrm{j}k_{z,e}d_e})}\right]\mathrm{d}(k_\rho^2)$$
$$+ \int_0^\infty \Re\left[\frac{3(1 + r^{\mathrm{TE}}_{e,M}\mathrm{e}^{2\mathrm{j}k_{z,e}z_+})(1 + r^{\mathrm{TE}}_{e,-N}\mathrm{e}^{2\mathrm{j}k_{z,e}z_-})}{8k_ek_{z,e}(1 - r^{\mathrm{TE}}_{e,M}r^{\mathrm{TE}}_{e,-N}\mathrm{e}^{2\mathrm{j}k_{z,e}d_e})}\right]\mathrm{d}(k_\rho^2). \quad (4)$$

Here $\Re[\cdot]$ stands for the real part of $[\cdot]$. k_ρ and $k_{z,e}$ are the radial and z components of the wave vector in cylindrical coordinates. $k_{z,i}$ in the ith layer ($i = M, \ldots, 1, e, -1, \ldots, -N$) is given by

$$k_{z,i} = (k_0^2 \varepsilon_i - k_\rho^2)^{1/2}, \tag{5}$$

where k_0 is the wave number in vacuum. We define $k_{z,i}$ in the first quadrant of the complex plane to ensure the radiation condition at infinity. Similarly, the normalized power U_{V} and U_{H} for VED and HED, respectively, transmitted to the region M can also be obtained as

$$U_{\mathrm{V}} = \int_0^\infty \frac{3\varepsilon_e k_\rho^2 |1 + r_{e,M}^{\mathrm{TM}} \mathrm{e}^{2\mathrm{j}k_{z,e}z_+}|^2 |t_{e,M}^{\mathrm{TM}}|^2 \Re\left[\frac{k_{z,M}}{\varepsilon_M}\right] \mathrm{e}^{-2\Im(k_{z,e})z_+}}{8k_e^3 |k_{z,e}^2| |1 - r_{e,M}^{\mathrm{TM}} r_{e,-N}^{\mathrm{TM}} \mathrm{e}^{2\mathrm{j}k_{z,e}d_e}|^2} \mathrm{d}(k_\rho^2), \tag{6}$$

$$U_{\mathrm{H}} = \int_0^\infty \frac{3\varepsilon_e |1 - r_{e,M}^{\mathrm{TM}} \mathrm{e}^{2\mathrm{j}k_{z,e}z_+}|^2 |t_{e,M}^{\mathrm{TM}}|^2 \Re\left[\frac{k_{z,M}}{\varepsilon_M}\right] \mathrm{e}^{-2\Im(k_{z,e})z_+}}{16k_e^3 |1 - r_{e,M}^{\mathrm{TM}} r_{e,-N}^{\mathrm{TM}} \mathrm{e}^{2\mathrm{j}k_{z,e}d_e}|^2} \mathrm{d}(k_\rho^2) + \int_0^\infty \frac{3|1 + r_{e,M}^{\mathrm{TE}} \mathrm{e}^{2\mathrm{j}k_{z,e}z_+}|^2 |t_{e,M}^{\mathrm{TM}}|^2 \Re[k_{z,M}] \mathrm{e}^{-2\Im(k_{z,e})z_+}}{16k_e |k_{z,e}^2| |1 - r_{e,M}^{\mathrm{TE}} r_{e,-N}^{\mathrm{TE}} \mathrm{e}^{2\mathrm{j}k_{z,e}d_e}|^2} \mathrm{d}(k_\rho^2). \tag{7}$$

Here $\Im(\cdot)$ stands for the imaginary part of $(\cdot)$. For a randomly oriented dipole with equal probability for all directions in space, we have

$$F_{\mathrm{R}} = \tfrac{1}{3} F_{\mathrm{V}} + \tfrac{2}{3} F_{\mathrm{H}} = \tfrac{1}{3} F_{\mathrm{V}}^{\mathrm{TM}} + \tfrac{2}{3} (F_{\mathrm{H}}^{\mathrm{TE}} + F_{\mathrm{H}}^{\mathrm{TM}}), \tag{8}$$

$$U_{\mathrm{R}} = \tfrac{1}{3} U_{\mathrm{V}} + \tfrac{2}{3} U_{\mathrm{H}} = \tfrac{1}{3} U_{\mathrm{V}}^{\mathrm{TM}} + \tfrac{2}{3} (U_{\mathrm{H}}^{\mathrm{TE}} + U_{\mathrm{H}}^{\mathrm{TM}}), \tag{9}$$

where the superscripts TE and TM denote the TE and TM modes, respectively. With the consideration of the Purcell effect, the angular power density $s(\alpha)$ in the region M can be expressed from the transmitted power of equation (2):

$$s(\alpha, \lambda) = \varepsilon_M k_0^2 \cos\alpha U_{\mathrm{R}} (k_0 \varepsilon_M^{1/2} \sin\alpha) / \pi [1 + (F_{\mathrm{R}} - 1)\eta_{\mathrm{int}}^0], \tag{10}$$

by assuming ε_M is real where k_0 is the wave number in vacuum and η_{int}^0 is the internal quantum efficiency of the bulk emitting material. The emission spectrum can be determined as

$$I(\alpha, \lambda) = s(\alpha, \lambda) L(\lambda), \tag{11}$$

where $L(\lambda)$ is the intrinsic spectrum of the emissive materials. The refractive indices of glass, Alq_3 and NPD are taken from [20, 21]. The complex permittivity of ITO, Ag and Al is taken from [22].

3. Results and discussions

The results of Device A with no Ag layer are shown in figure 2(*a*). The spectra are normalized to the sharp red peak of the $Eu(DBM)_3$bath at 620 nm for intuitively showing the changes. At a low bias, the sharp red emission of the $Eu(DBM)_3$bath at 620 nm is obtained. When the bias is increased, the emission from NPD and exciplex enhances and gradually dominates the emission. The tuning of the emission colour can be explained by two factors. The first one is the efficiency reduction of the $Eu(DBM)_3$bath when the applied voltage is high. This reduces the red emission of the $Eu(DBM)_3$bath and blue from NPD dominates the emission. The other is the extension of the recombination zone in the device and thus the red emission exists at high voltages. As a result, a colour-tunable OLED from red to white is obtained. However, the broad emission of NPD and exciplex prevents the colour tuning from reaching the primary colour.

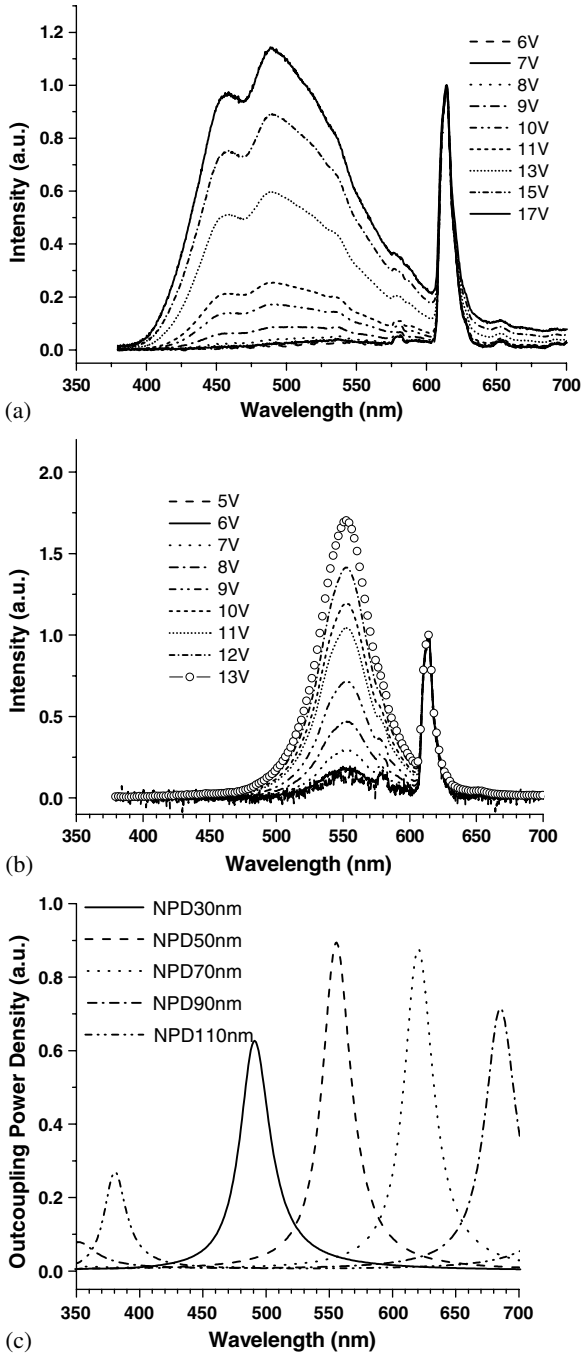

Figure 2. The emission spectrum of Device A (*a*) without an Ag layer and (*b*) with Ag layer of 40 nm. All EL spectra are normalized to the Eu peak at 615 nm for comparison. (*c*) The zero degree outcoupling power density of the cavity structure with 40 nm Ag layer and various NPD thicknesses.

The introduction of the Ag layer into Device A forms a cavity structure with Al so that the broad emission can be

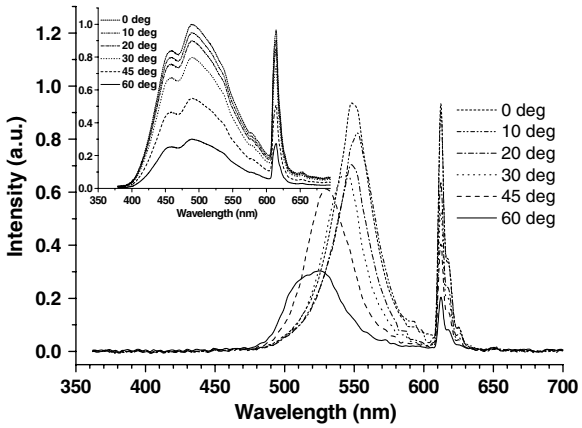

Figure 3. The emission spectrum of Device A biased at 10 V at different viewing angles.

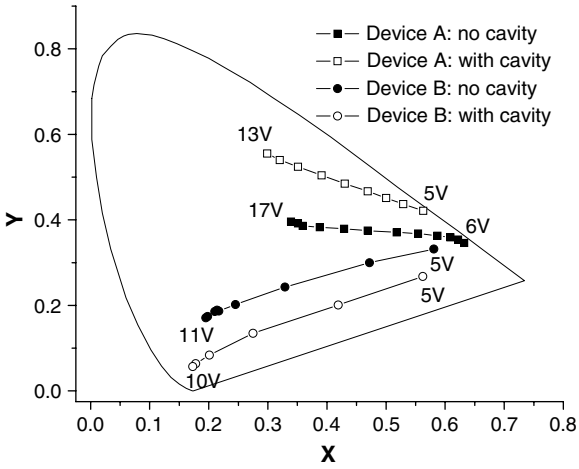

Figure 4. The CIE chromaticity diagram of Devices A and B with and without an Ag layer.

narrowed down. From the modelling results, the cavity resonance wavelength at zero degree (normal to the device surface) for the case of Device A with 40 nm of Ag and 50 nm of NPD is at about 550 nm as shown in figure 2(*c*). Increasing the thickness of the Ag layer can further narrow down the resonance spectrum and improve the colour purity. However, the red emission of the $Eu(DBM)_3$bath will be degraded. Therefore, there is a tradeoff between the red emission intensity and the colour purity of the resonance wavelength at 550 nm. The optimized experimental result of 40 nm of Ag is shown in figure 2(*b*). With the microcavity effects, the broad emission of NPD and exciplex with full-width-half-maximum (FWHM) over 120 nm is significantly reduced by 2.5 times to about 50 nm. The emission spectra of Device A with the Ag layer biased at 10 V at different viewing angles are shown in figure 3. It can be seen that due to the microcavity effect, the spectrum blue shifts when the spectra of Device A without Ag do not have any obvious shift as shown in the inset of figure 3. As shown in figure 2(*b*), the peak wavelength is at 550 nm and in good agreement with the modelled results. The brightness of the device reaches about 600 $Cd\,m^{-2}$. The current efficiency at a low current density is about 3 $Cd\,A^{-1}$. By optimizing the material and device structure, it has been reported that the current efficiency of $Eu(DBM)_3$bath OLEDs could reach $\sim$4 $Cd\,A^{-1}$ [23]. It has been reported that the brightness and current efficiency can be improved by codoping an Eu material with a fluorescent dye of 4-(dicyanomethylene)-2-t-butyl-6(1,1,7,7-tetramethyljulolidyl-9-enyl)-4H-pyran (DCJTB) [24]. Consequently, colour-tunable OLEDs from red to green with enhanced colour purity are achieved. The CIE coordinates of the emission of Device A can be determined from the spectra in figure 2 and the results are plotted as shown in figure 4. The whole colour tuning route moves towards the boundary of the CIE chromaticity diagram with a more saturated colour than the device without the cavity.

Conventionally, the destination colour of the tunable OLED can be modified by doping NPD with dyes. Here, our aim is to engineer the colour-tunable OLED of Device A from red-to-green to become a red-to-blue tunable OLED without adding any other organic materials to the device structure. As shown in figure 5, we can achieve the red-to-blue tunable OLED by reducing the thickness of the device to Device B: ITO/Ag(40 nm)/CuPc(10 nm)/NPD(x nm)/$Eu(DBM)_3$bath (15 nm)/Alq_3 (25 nm)/LiF (0.5 nm)/Al (150 nm).

Figure 5(*c*) shows the modelling results when the thickness of NPD increases, the resonant wavelength red shifts and beyond the visible wavelength range when the thickness is thicker than 100 nm. The resonant peak cycles periodically such that when the NPD thickness is further increased to 140 nm, the resonance peak is at 388 nm. The magnitude of the zero degree outcoupling power density considerably reduces when the NPD thickness is less than 20 nm because the electric dipole is too close to Ag and the power is absorbed by the Ag layer. Using the NPD thickness of 40 nm, the resonant wavelength reaches about 450 nm. As shown in figure 5(*b*), the blue emission spectrum is considerably narrower as compared with the one without the Ag layer (figure 5(*a*)) and the colour tuning route therefore moves towards the bottom boundary of the CIE chromaticity diagram of figure 4 with purer spectrum colour.

It should be noted that microcavity structures may result in a large angular dependence on the emitting colour, which causes problems for display applications. However, several methods have been actively investigated to address the viewing angle issues such as introduction of colour filtration [25] and structures with a dispersive refractive index [26–28] to reduce the spectral shift with a viewing angle.

4. Conclusion

Theoretical and experimental investigation of the emission spectrum of single-unit voltage-controlled colour-tunable OLEDs has been conducted in this paper. While colour purity is a concern in typical single-unit tunable OLEDs, our results show that microcavity structures can improve not only the destination colour but also the whole colour-tunable route towards saturated colour. With the studies on the periodical cycling of resonant wavelength and absorption loss of metal electrodes, the destination colour has been engineered by modifying the cavity thickness without adding any dyes to colour-tunable OLEDs.

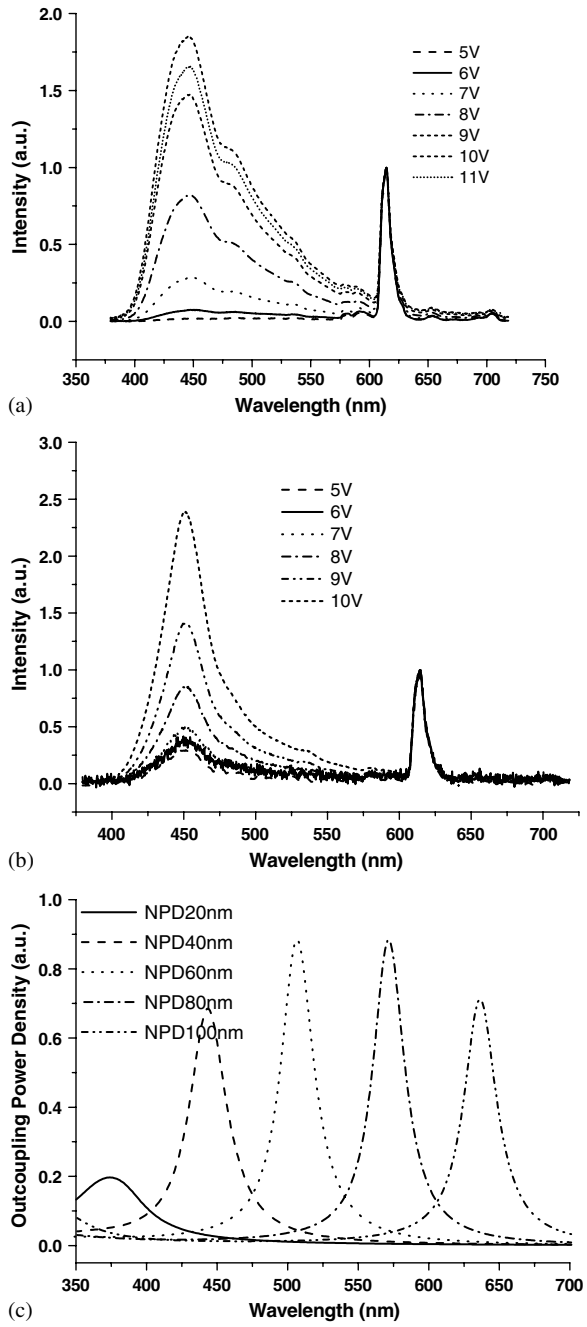

Figure 5. The emission spectrum of Device B (*a*) without an Ag layer and (*b*) with an Ag layer of 40 nm. All the EL spectra are normalized to the Eu peak at 615 nm for comparison. (*c*) The zero degree outcoupling power density of the cavity structure with 40 nm Ag layer and various NPD thicknesses.

Acknowledgments

The authors would like to acknowledge the support of the UDF Grant, the Strategic Research Grant in organic optoelectronics of the University of Hong Kong and the Grant (#14300.324.01) from the Research Grant Council of the Hong Kong Special Administrative Region, China.

References

[1] Burrows P E, Forrest S R, Sibley S P and Thompson M E 1996 *Appl. Phys. Lett.* **69** 2959
[2] Gu G, Khalfin V and Forrest S R 1998 *Appl. Phys. Lett.* **73** 2399
[3] Shen Z, Burrows P E, Bulovic V, Forrest S R and Thompson M E 1997 *Science* **276** 2009
[4] Yoshida M, Fujii A, Ohmori Y and Yoshino K 1996 *Appl. Phys. Lett.* **69** 734
[5] Kalinowski J, Di Marco P, Cocchi M, Camaioni N and Duff J 1996 *Appl. Phys. Lett.* **68** 2317
[6] Reyes R, Cremona M, Teotonio E E S, Brito H F and Malta O L 2004 *Chem. Phys. Lett.* **396** 54
[7] Granstrom M and Inganas O 1996 *Appl. Phys. Lett.* **68** 147
[8] Wang Y Z, Sun R G, Meghdadi F, Leising G and Epstein A J 1999 *Appl. Phys. Lett.* **74** 3613
[9] Huang C C, Meng H F, Ho G K, Chen C H, Hsu C S, Huang J H, Horng S F, Chen B X and Chen L C 2004 *Appl. Phys. Lett.* **84** 1195
[10] Chen X W, Choy W C H and He S 2007 *IEEE J. Display Technol.* **3** 110
[11] Choy W C H and Li E H 1997 *IEEE J. Quantum Electron.* **33** 382
[12] Adawi A M, Connolly L G, Whittaker D M, Lidzey D G, Smith E, Roberts M, Qureshi F, Foden C and Athanassopoulou N 2006 *J. Appl. Phys.* **99** 054505
[13] Crawford O H 1989 *J. Chem. Phys.* **89** 6017
[14] Bulovic V, Khalfin V B, Gu G, Burrows P E, Garbuzov D Z and Forrest S R 1998 *Phys. Rev.* B **58** 3730
[15] Neyts K, Visschere P D, Fork D K and Anderson G B 2000 *J. Opt. Soc. Am.* B **17** 114
[16] Liang C J and Choy W C H 2006 *Appl. Phys. Lett.* **89** 251108
[17] Fong H H, Choy W C H, Hui K N and Liang Y J 2006 *Appl. Phys. Lett.* **88** 113510
[18] Lukosz W 1980 *Phys. Rev.* B **22** 3030
[19] Neyts K 1998 *J. Opt. Soc. Am.* A **15** 962
[20] Masenelli B, Callard S, Gagnaire A and Joseph J 2000 *Thin Solid Films* **364** 264
[21] Choy W C H and Fong H H 2007 *J. Appl. Phys.* submitted
[22] Hobson P A, Wasey J A E, Sage I and Barnes W L 2002 *IEEE J. Sel. Top. Quantum Electron.* **8** 378
[23] Hong Z *et al* 2001 *Adv. Mater.* **13** 1241
[24] Fang J, You H, Gao J and Ma D 2004 *Chem. Phys. Lett.* **392** 11
[25] Lidzey D G, Pate M A, Whittaker D M, Bradley D D C, Weaver M S, Fisher T A and Skolnick M S 1996 *Chem. Phys. Lett.* **263** 655
[26] Tessler N, Burns S, Becker H and Friend R H 1997 *Appl. Phys. Lett.* **70** 556
[27] Hou L, Hou Q, Peng Y and Cao Y 2005 *Appl. Phys. Lett.* **87** 243504
[28] Choy W C H and Ho YC 2007 *Opt. Express* **15** 13288